Natural Rail Surface Defect Inspection and analysis using 16-channel Eddy Current System

Segon Kwon [1], Taekgyu Lee [2], Sangjun Park [3], Jeongwon Park [4] , and Jong-Min Seo [1,*]

1 Technology Research Department, KORAIL Research Institute, Daejeon, Republic of Korea
2 Shalom engineering co, Jungwon-gu, Seongnam, Gyeonggi-do, Republic of Korea
3 Twotrack co, Osong-eup, Heungdeok-gu, Cheongju-si, Chungcheongbuk-do, Republic of Korea
4 KRISS, Gajeong-ro, Yuseong-gu, Daejeon, Republic of Korea
* Correspondence: seojm@korail.com; Tel.: +82-042-615-5218

Received: date; Accepted: date; Published: date

Abstract: Trains are used by many as the fastest mode of transportation between countries and land. In order to operate a train, it is moved along a special road called a 'rail'. Rail is the number of train movement and fatigue and the accumulation, since the corrosion rate of the rail due to the environment is very high, it is necessary ongoing safety. Researchers have actively investigated and developed rail defect inspection systems employing non-destructive techniques to address these problems. In particular, the eddy current inspection technique does not involve contacting with the surface of the test specimen and offers the advantage of excellent rail defect detection sensitivity. Therefore, a 16Ch Array eddy current inspection device was developed to inspect the surface defects of the rail. An equation was derived to predict the correlation between the depth and phase of an artificial defect using an eddy current inspection device, and the equation derived from natural defect was applied.

Keywords: Railway; Eddy current; Surface defect; Array system

1. Introduction

Trains are the fastest means of transportation on land, contributing greatly to industrial development. Railway tracks are required for trains to move, and rails are composed of supports, sleepers, and roadbeds to distribute the train's load. These rails are constantly subjected to fatigue load due to friction with the wheels of the train, and defects in the rail occur due to corrosion caused by the external environment (climate, etc.) [1]. Various surface defects in rails occur most frequently during rolling stock operation, and internal defects may develop which leads to accidents if maintenance such as grinding is insufficient or not performed in advance.

In general, a visual inspection method is used for inspecting rail defects. As a method for inspectors to walk around and check whether or not a defect has occurred in the rail, visual inspection is possible to easily perform defect inspection even without proficiency. However, in land transport inspection, it is difficult to determine defects occurring inside the rail, and there is a limit to the area that can be inspected. Another non-destructive method of detecting defects is ultrasonic flaw detection.

Ultrasonic flaw detection is a method of inspecting the inside of a rail with a wave generated by vibrating a specific material [2-3]. Inspection using ultrasound has developed to the stage where it is possible to check the inside of the rail in the form of an image using phased arrays, but it has a disadvantage in that it is difficult to detect defects on the surface of the rail due to the flaw detection structure. In particular, it is impossible to detect a squat-type defect that occurs on the rail surface because the ultrasonic wave does not propagate due to the instantaneous void between the rail surface and the ultrasonic probe surface.

Eddy current flaw detection is a technique proposed to compensate for the shortcomings of visual inspection and ultrasonic inspection. The eddy current inspection technique is a non-contact method in which a high-frequency alternating current is applied to generate a magnetic field to detect changes in impedance between a coil and specimen, or changes in voltage induced in a coil [4-6].

Therefore, eddy current inspection can be used to inspect the inside of the rail, which is a disadvantage of visual inspection, and can be used very usefully because it can inspect the surface area, which is a disadvantage of ultrasonic inspection [7~8]. In the eddy current inspection method, a Lissajous figure can be drawn using X data (resistance) and Y data (reactance), which are signals output from the sensor, and the size of a defect can be obtained using amplitude and phase [9-10].

The currently developed eddy current flaw detection equipment is designed in a structure that cannot inspect the entire head of the rail using a small number of sensors. In order to inspect the entire head of the rail, a technology that can minimize the dead zone area using multiple eddy current sensors is required. Along with the minimization of the dead band region, the performance of the eddy current sensor also plays an important role. In general, an eddy current sensor consists of a coil, and since a coil that responds according to the direction of a defect is determined, a technology capable of inspecting all defects using one sensor is required.

In this study, the number of sensors was optimized by manufacturing a Plus-Point coil so that flaw detection can be performed regardless of the direction of the defect, and a total of 16 eddy current sensors were used to inspect the entire head of the rail. In addition, two-dimensional and three-dimensional rail surface shapes was obtainable through separate software, and a relational expression for analyzing the depth of the defect was derived by manufacturing artificial defects on the rail surface.

2. Defect detection technique using multi-channel eddy current system

The multi-channel eddy current inspection system developed in this study was applied to investigate natural surface defects on a UIC 60 rail. Obtained signals were used to compare and evaluate the signal characteristics of the defects and compare them with the actual defects in 2D and 3D images to confirm the accuracy of the defect detection.

Fig. 1 displays the analysis sequence for multi-channel eddy current testing. The X and Y data of natural rail defect test specimens are collected using a multi-channel sensor, and the data is subsequently subjected to a de-trending and de-noising process. It is possible to acquire the defect image after correcting the difference (amplitude, phase) between the sensors. The respective procedure is described in detail below in Figure 1.

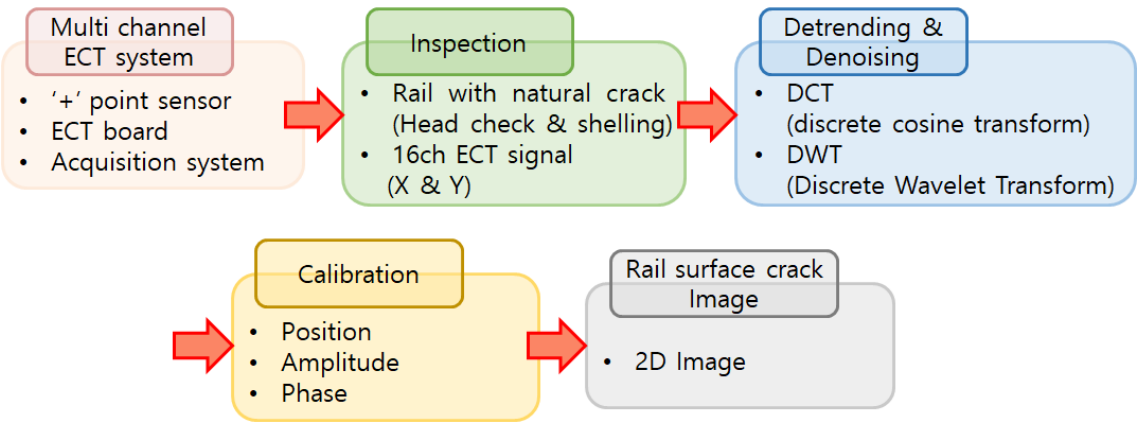
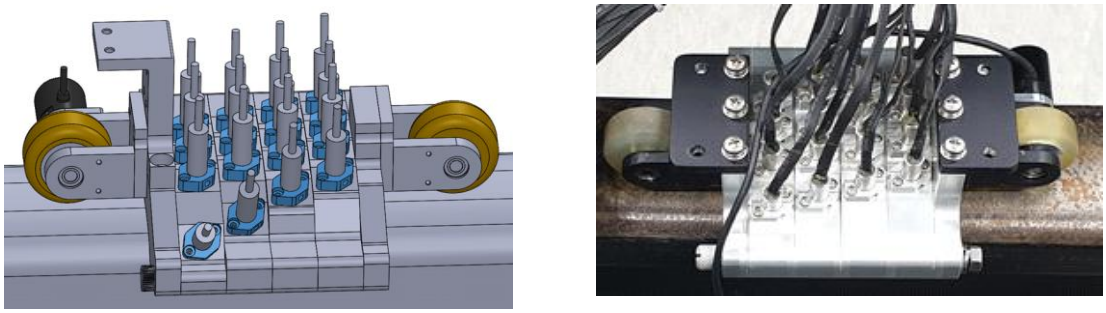


Figure 1. Multi-channel ECT signal analysis

2.1 16ch eddy current sensors

Plus-point sensors which are types of differential sensors were used in this study [11]. The plus-point sensors cross the "I"-shaped coils crosswise to differentially detect the defects; as the lift-off (gap between the specimen and sensor) changes, the crossed coils are simultaneously affected and canceled, thus minimizing the effect of lift-off and reducing noise [12-13]. Furthermore, defects in various directions rather than in one direction can be detected [14]. The plus-point sensors were fabricated with four layers (two layers each) with an outer diameter of 8 mm and a high of 30mm.



(a) (b)

Figure 2. Multi-channel ECT sensor jig

The jig was constructed as shown in Figure 2 (a), (b) such that the 16 sensors could be secured and such that the entire rail surface could be inspected. The sensor spacing in the direction of rail propagation is set to 18mm, and to inspect the entire rail head, the sensor spacing between the rail propagation direction and vertical direction is 3.8mm, which comes to a total of 57mm. The jig to which the sensors were connected was divided into four parts and could be disassembled and reassembled. Four sensors were combined onto one jig apparatus, and the arrangement of the sensors could be changed by disassembling and reassembling the jig. Furthermore, a constant lift-off distance from the wheels attached to the jig to the rail surface could be maintained.

2.2 16ch Eddy Current System

2.2.1 System Introduction

A power supply was used to apply 12V of power to the 16-channel eddy current system. The 16 channel eddy current system distributes the supplied power and applies 7V of power to the sensors; connected to the acquisition program through LAN connection, and stores the real-time monitoring data and outputs X and Y component signals. The acquisition program can monitor 16 channels of X and Y signals and 2D images in real time, and can create a 3D image of the section where a defect occurs. In addition, the frequency and gain value can be set. In the experiment, we applied a frequency of 300 kHz and a lift-off of 1mm.

2.2.2 Frequency setting

In order to set the optimal frequency of the multi-channel eddy current system, the phase change was confirmed according to the frequency change as shown in Table 1. When the amount of phase change is large, the resolution increases when converted to the depth of the defect, and the error of the defect decreases as the deviation value becomes minimum in the same defect. It was confirmed that the frequency change amount was measured the largest at 300 KHz, and the deviation was minimum at 350 & 300 KHz. Therefore, the optimum frequency, 300 KHz, was set as the optimum frequency for measuring defects.

Table 1. Phase change according to frequency change

Frequency	Phase (°)	Diff.

(KHz)	Experiment No.	2	4	6	8	10	
350	1	-32.4524	-30.3850	-29.2999	-29.1240	-28.3642	4.0882
	2	-32.6870	-29.8540	-28.0738	-28.0546	-27.6734	5.0135
	3	-32.3204	-30.0768	-27.8388	-28.2921	-27.4583	4.8621
320	4	-30.4027	-28.1381	-26.3929	-26.4434	-25.8961	4.5066
	5	-30.5754	-28.6660	-26.4390	-27.0946	-25.9125	4.6629
	6	-30.4502	-29.2462	-28.2148	-28.8166	-27.9754	2.4748
300	7	-28.6188	-26.7763	-25.4320	-25.1339	-24.9633	3.6555
	8	-28.9136	-26.3983	-24.1699	-24.3644	-23.6386	5.2750
	9	-29.0956	-26.2600	-24.1791	-23.7882	-23.1767	5.9189
280	10	-27.1936	-23.6182	-21.9481	-21.4577	-20.9467	6.2469
	11	-27.4504	-24.5873	-22.3666	-22.4646	-21.9302	5.5202
	12	-26.6520	-24.8633	-24.8383	-25.2977	-24.2320	2.4200
250	13	-21.4763	-20.1548	-19.1546	-20.0823	-18.7823	2.6939
	14	-23.0456	-20.2948	-19.5484	-18.8781	-18.2876	4.7579
	15	-23.3839	-20.7719	-19.5402	-20.0642	-18.9385	4.4454

2.3 Natural crack specimen

Natural defects occur due to rolling stock operation on the rail and cumulative tonnage (more than 500 million tons) and external environmental factors. Natural defects that occur in general are shown in Figure 5 (a) and (b). Figure 5 (a) shows a head check defect on the rail surface, and Figure 5 (b) shows a shelling defect on the rail surface.

The head check occurs as a solid line owing to slip and frictional stress between the rail and wheel [15-16]. Shelling occurs due to the development of head check; it is a defect in which the surface of the rail breaks shallowly owing to the continuous load and friction of the train.



(a) (b)

Figure 5. Crack specimen : (a) Head check, (b) Shelling

2.4 Calibration data

2.4.1 Calibration Specimen

This study aims to measure the defects occurring in the rail head using a 16ch eddy current sensor. However, since the 16ch eddy current sensor is manufactured by hand, a difference occurs in the amplitude measured by the sensor when passing through the same defect. In order to minimize the error between the sensors, a calibration test piece as shown in Figure 6 was prepared. In order to ensure that all sensors pass through the same defect, the calibration test piece was manufactured with a defect having a length of 1 mm and a depth of 3 mm over the entire head.

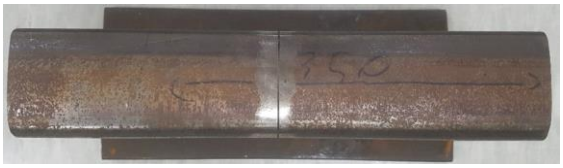
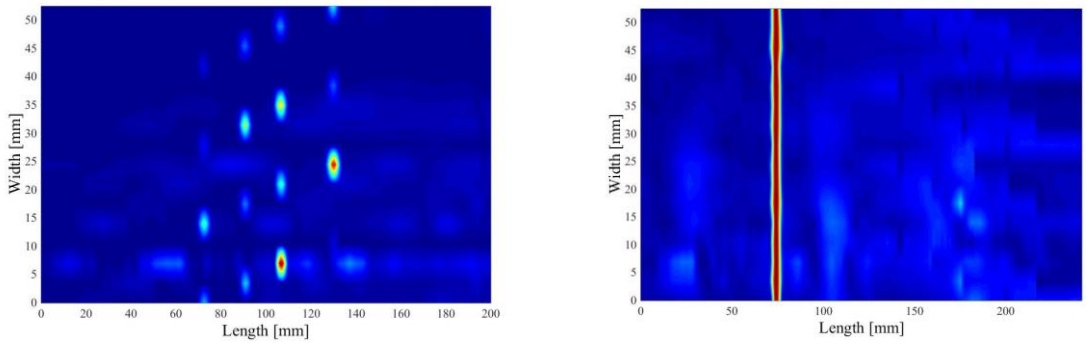


Figure 6. Calibration Specimen

As shown in Figure 2 does not have the sensor lies on a straight line, are arranged in an array of 4 X 4. Therefore, when scanning the test piece in Figure 6 can obtain the results shown in Figure 7 (a). Since the actual defect lies on a straight line, position correction is required, and a calibration value that minimizes the amplitude difference between sensors is required.

- Calibration value measurement method (position & amplitude)
  1) Check the defect location of each sensor.
  2) The sensor number that found the defect first is called "A1".
  3) The distance difference from each sensor to "A1" is called the position calibration value.
  4) Check the amplitude of each sensor.
  5) The sensor number with the maximum amplitude is called "B1".
  6) The value multiplied so that the amplitude of each sensor becomes "B1" is called the amplitude calibration value.

Fig. 7(b) is the result of applying the calibration value, and it can be confirmed that all have the same amplitude at the same location.



(a) (b)

Figure 7. Calibration : (a) Before, (b) After.

2.4.2 Signal Processing (Denoising & Detrending)

Fig. 8 is raw data of 16ch eddy current sensor passing the calibration test piece in Fig. 6. Since only one defect exists in the calibration test piece, the amplitude change occurs once for each sensor. It can be seen that there is a difference in amplitude depending on the characteristics of each sensor, and it can be seen that sensors 4 & 8 generate a lot of noise.

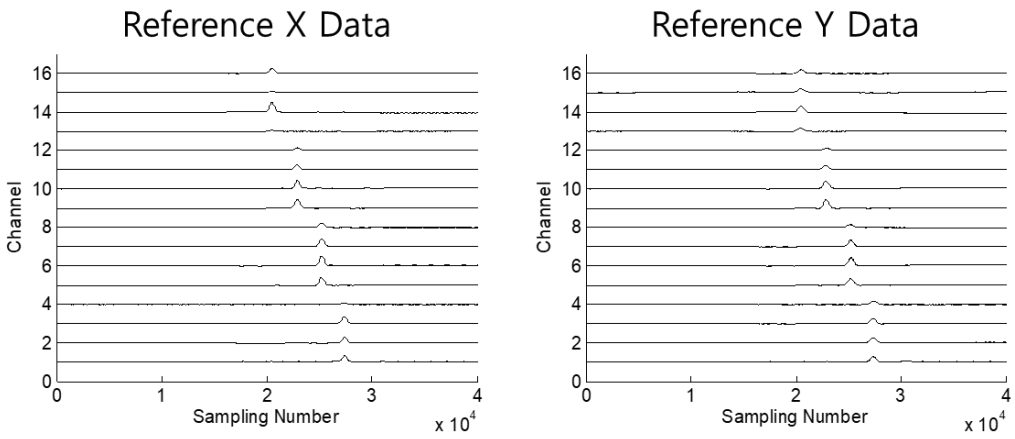


Figure 8. Reference data

Since the noise of the signal cannot find the location of the defect or acts as an error in analyzing the size of the defect, noise removal is performed through denoising. The denoising technique used in this study is "DC Offect", and signal processing is performed by applying data between the initially generated low frequency and a specific high frequency. Fig. 9 shows the denoising process, and it can be confirmed that noise disappeared as a result of applying "DC Offect".

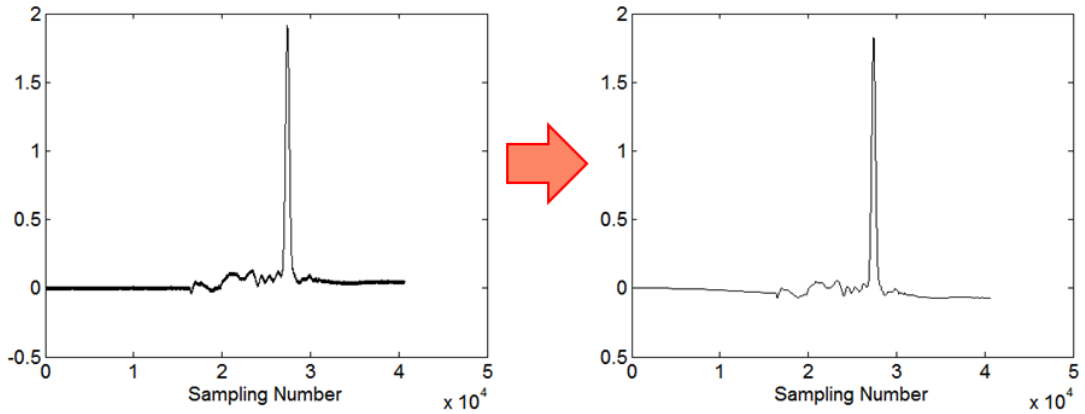


Figure 9. Denoising process

As can be seen in Figure 9, it can be seen that the denoising data has a certain tendency. Certain trends can also be viewed as noise, and Detrending removes certain trends in data. In this study, "Polynominal Fitting – Bisquar & Givens" technique was used for detrending. Fig. 10 shows the process of detrending the data of Ch4 after the denoising process.

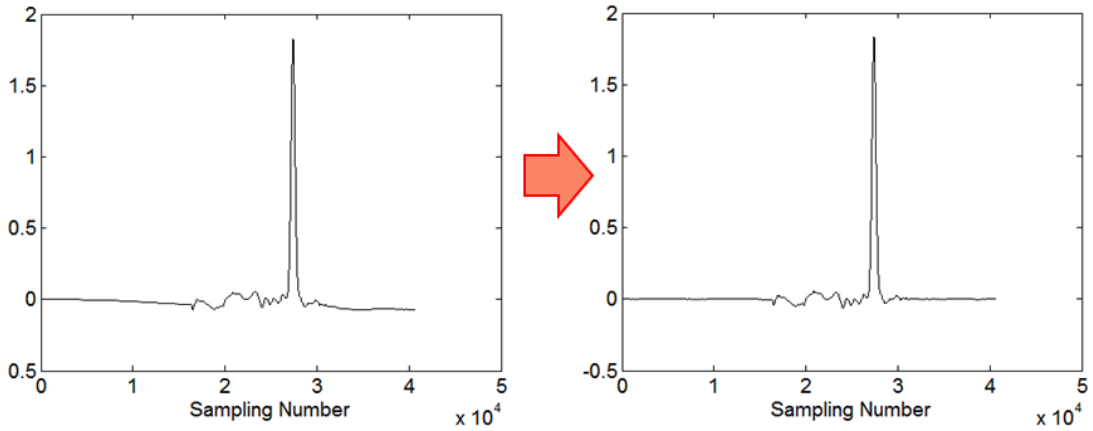


Figure 10. Detrending process

2.4.3 Cali Signal Correction using Calibration Test Specimens

Table 2 shows the position, amplitude and phase of the sensor from the calibration data obtained from Figure 10. The position was adjusted so that all defect signals could be acquired from the same position. Amplitude is the correction value used to make all sensors the same as they go through the same defect. Phase must also have the same angle because all sensors go through the same defect. The angle was set so that all sensors were set to 45°.

Table 2. Calibration data set

Sensor No.	Position	Amplitude	Phase
1	2	0.402508	17.11275
2	107	0.62523	19.17356
3	198	0.167484	16.6256
4	331	0.131602	-19.8094
5	2	0.46426	18.30923
6	106	0.329545	14.72798
7	198	0.77161	14.66705
8	331	0.300235	27.22918
9	1	1.414214	6.24507
10	106	0.601665	14.87781
11	197	0.919032	18.81284
12	330	0.355008	22.96367
13	0	0.112376	-33.8415
14	105	1.287556	20.83283
15	196	0.281211	-14.1919
16	330	0.509686	20.42483

3. Depth Estimation of artificial and natural defects

3.1 Multi-Channel Eddy Current System for Rail Surface Defect Inspection

In order to carry out the inspection at a long distance in the field, an equipment as is shown in Figure 11 was manufactured. The multi-channel sensor has 16 transducer channels built in, where the system is equipped power and sensor for collecting signals, and the Acquisition Program can be installed on a tablet PC to lighten the equipment. The inspection speed of the equipment was set to 2 km/h, compliant to the average walking speed of ordinary people.



Figure 11. Equipment used in the field

3.2 Depth estimation using artificial defect specimen

In order to derive the relationship between the depth and the phase of the defect, in Figure 12 the artificial defect specimen was made with four squat defects on the UIC60 sample. The depth of the defect was 2, 4, 6, and 8 mm, and the length and width were 10 mm.

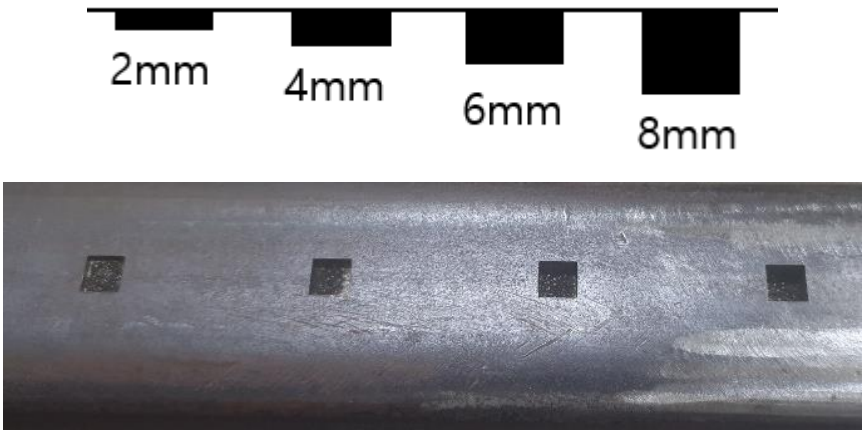
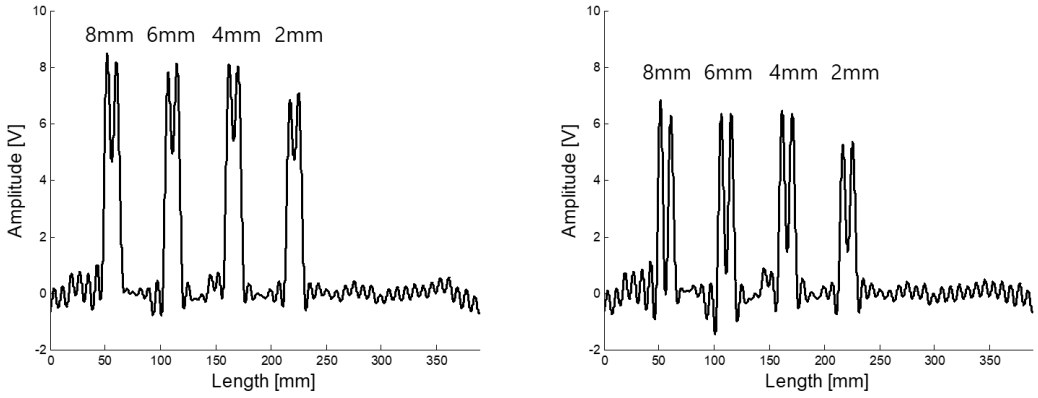


Figure 12. Artificial defect depth change specimen

Figure 13 shows the results of the scan of the artificial defect specimen. Figure 13(a) is the X data (Resistance) of the 8th sensor, and Figure 13(b) is the Y data (Reactance). In Figures (a) and (b), Detrending & Denoising were performed through signal processing. As a result of applying calibration, it was confirmed that two peaks are generated when the detector passes the defect. These two peaks are the start and end points of the defect, and the length of the defect can be measured through the two peak points.



(a) (b)

Figure 13. Ch 8 Data (a) X data (Resistance), (b) Y data (Reactance)

Phase is used to estimate the depth of the defect. Figure 14 shows the relationship for estimating the depth of defects, and Equation (2) shows the relationship between depth and phase. As a result of the measurement, it was confirmed that the phase increases at a constant rate as the depth of the defect increases. It can be confirmed that there is no problem in the sensor and system of this experiment by constantly changing the phase as the depth changes.

$$\text{Depth} = 1.5593 \times \text{Phase} - 57.864 \quad (2)$$

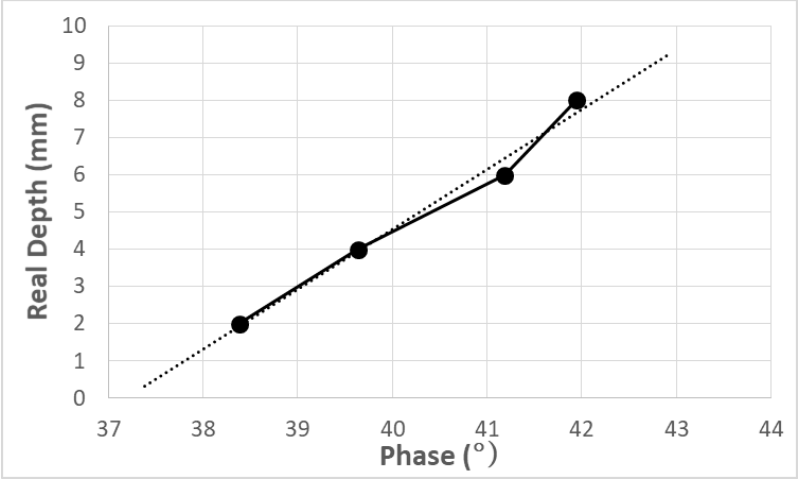


Figure 14. Correlation between depth and phase

Figure 15 shows the results of estimating the depth of artificial defects according to the depth change through a total of 6 repeated experiments. The red dotted line in Figure 15 is an error bar of ±1mm, and it can be observed that there is no point beyond the error bar. Therefore, it is possible to estimate the depth of surface defects of different specimens using the correlation between the depth and the phase of the derived defect.

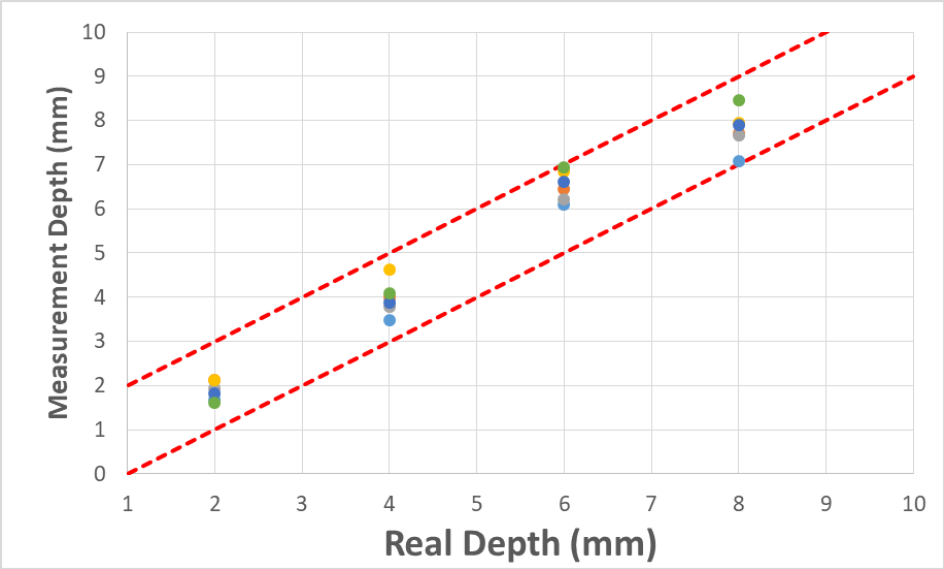


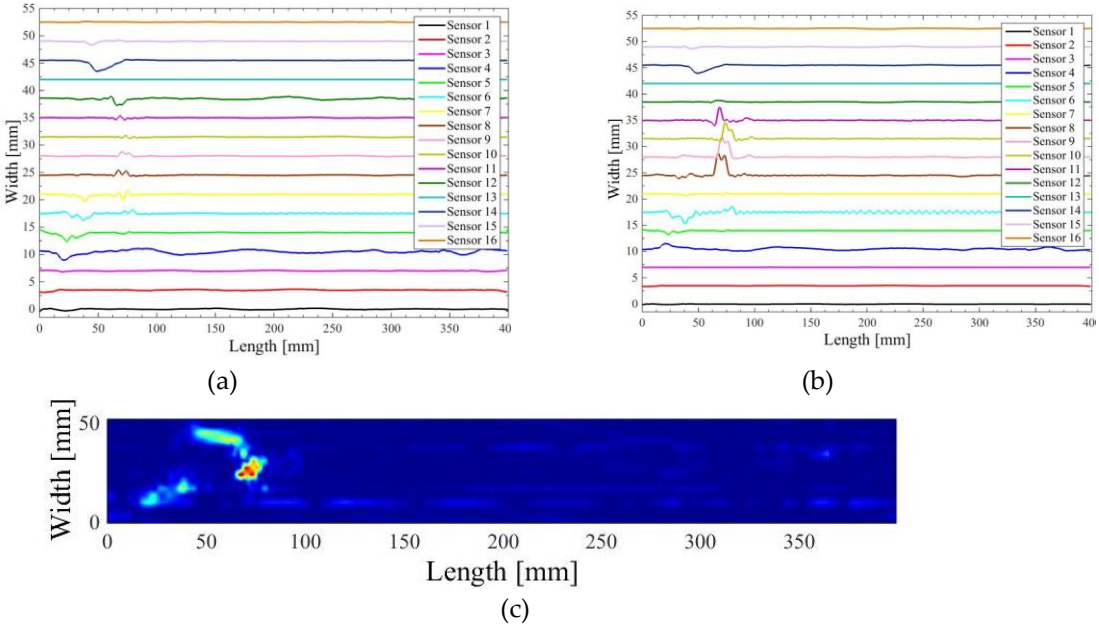
Figure 15. Depth estimation result of artificial defect specimen

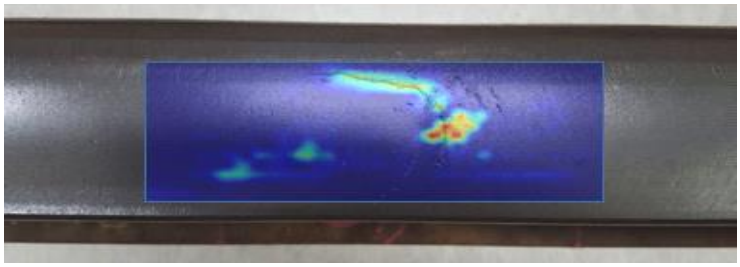
3.3 Natural Rail Defect Test Specimen Image

By applying the calibration data in Table 1, the head check defect inspection of Figure 5 (a) results using the 16 channel sensors are shown in Figure 16. Figure 16 (a) is X data (Resistance), and Figure 16 (b) is Y data (Reactance). In Figure 16 (a) and (b), the depth of the head check defect can be expected to vary because the X and Y signals are measured differently.

Figure 16 (c) shows an image similar to the shape of the specimen as the result of calibration. Figure 16 (d) is used for an exact comparison, by overlaying the defect part in Figure 16 (c) with the image of the actual defects and results were shown to be consistent with head check defects.

The measurement was conducted a total of 6 times using a 16ch array eddy current device, and the average value of the phases was measured to be 40.153 °. As a result of calculating by substituting the measured phase into Equation (2), the depth of the defect is 4.747 mm.

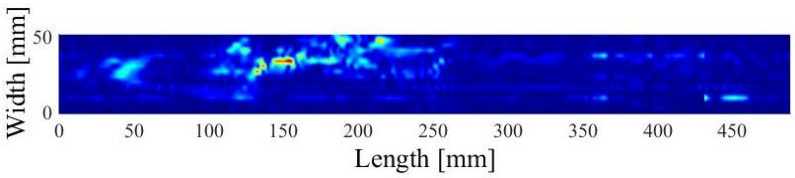




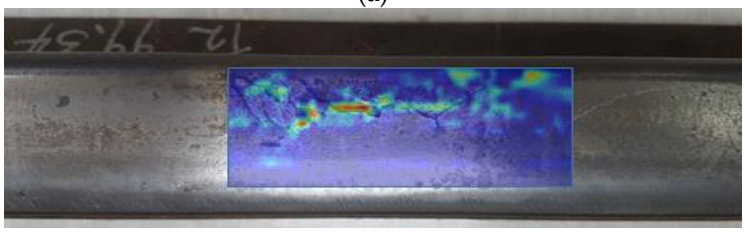
(d)

Figure 16. Head check signal using 16ch array ECT sensor : (a) X data (Resistance), (b) Y data (Reactance), (c) 2D, (d) Real & Result crack

Figure 17 (a) shows the image results after the shelling defect from Figure 5 (b) was calibrated. Figure 17 (b) is used for an exact comparison by overlaying over the image Figure 17 (a) with the actual defect and the deep-pitched position is measured to be at a similar point (but not at the precise same position. The measurement was conducted a total of 6 times using a 16ch array eddy current device, and the average value of the phases was measured to be 41.248 °. As a result of calculating by applying the measured phase to Equation (2), the depth of the defect is 6.454 mm.



(a)



(b)

Figure 17. Shelling signal using 16ch array ECT sensor : (a) X data (Resistance), (b) Y data (Reactance), (c) 2D Image

4. Conclusions

In this study, an artificial defect was installed on the UIC60 rail surface, and using a 16-channel eddy current flaw detection system, a relational equation to analyze the depth was derived. In addition, two-dimensional and three-dimensional defect images could be acquired using the newly developed program.

Sensor calibration and signal processing techniques were used to improve the inspection accuracy and signals. The comparison of signal characteristics indicated that the peak width of the head check defect was narrower than shelling defect. Two defects types (head check and shelling) were reproduced in 2D images and the images were compared to the actual defects. The location and distribution of the defect signals in the images overlapped with those of the actual defects. Furthermore, the position of the defect and the part in which the defect propagated in the depth direction were confirmed, which could not be confirmed visually in the previous stages. The 3D images of the defects allowed us to confirm the signal size of the section in which the depth had substantially increased, as well as the

surface roughness according to the degree of noise. The comparison of the 2D and 3D images using the 16-channel eddy current system with actual defects confirmed the detection accuracy.

Furthermore, to analyze the depth of defects, artificial defects were produced to derive the correlation between defects and phase. To confirm the reliability of the derived correlation, it can be confirmed that the error range does not exceed ±1mm through a number of experiments. It was confirmed that the depth can be analyzed using the correlation derived from the depth measurement of natural defects.

The 16-channel eddy current flaw detection equipment can be used to measure the defects on the rail surface, and it is expected to contribute to the stable management of the rail by applying it to 50K and 60K specimens.

References

1. S. W. Han, S. H. Cho (2011) Review of Non-Destructive Evaluation Technologies for Rail Inspection, Journal of the Korean Society for Nondestructive Testing, Vol. 31, No. 4, pp.398-413.
2. G. W. Kim, M. K. Seo, Y. I. Kim, S. G, Kwon, K. B. Kim (2020) Development of phased array ultrasonic system for detecting rail cracks, Sensors and Actuators A: Physical Vol. 311,
3. Thomas HECKEL, Hans-Martin THOMAS, Marc KREUTZBRUCK, Sven RÜHE (2009) High Speed Non-destructive Rail Testing with Advanced Ultrasound and Eddy-Current Testing Techniques, NDTIP Proceedings, Prague
4. Peng Xu, ChenLu Zhu, HongMing Zeng, Ping Wang (2020) Rail crack detection and evaluation at high speed based on differential ECT system, Measurement, Vol 166
5. Yating Yu, Kuanhou Gao, Bowen Liu, Linfeng Li (2020) Semi-analytical method for characterization slit defects in conducting metal by Eddy current nondestructive technique, Sensors and Actuators A: Physical, Vol 301
6. Mayorkinos P Papaelias, Martin Lugg (2012) Detection and evaluation of rail surface defects using alternating current field measurement techniques, Proceedings of the Institution of Mechanical Engineers, Part F: Journal of Rail and Rapid Transit, Vol. 226, Issue 5
7. J. W. park, J. H. Park, S. J. Song, M. B. Kishore, S.G. Kwon, H. J. Kim (2017) Enhanced Detection of Defects Using GMR Sensor Based Remote Field Eddy Current Technique, Journal of Magnetics , Vol. 22, No. 4, pp.531-538.
8. Javier Garcia-Martin, Jaime Gomez-Gil, Ernesto Vazquez-Sanchez (2011) Non-Destructive Techniques Based on Eddy Current Testing, Sensors, Vol. 11, No. 3, pp.2525-2565.
9. M Ph Papaelias, C Roberts, C L Davis (2008) A review on non-destructive evaluation of rails: State-of-the-art and future development, Proceedings of the Institution of Mechanical Engineers, Part F: Journal of Rail and Rapid Transit, vol. 222, Issue. 4, pp. 367-384.
10. J. W. Park, J. H. Park, S. J. Song, H. J. Kim, Se Gon Kwon (2016) GMR Sensor Applicability to Remote Field Eddy Current Defect Signal Detection in a Ferromagnetic Pipe, Journal of the Korean Society Nondestructive Testing, Vol. 36, No. 6, pp.483-489.
11. T. G. Lee, Y. T. Yeom, H. J. Kim, S. J. Song, S. G. Kwon, S. D. Kwon (2019) Analysis of Eddy Current Signal of Defects on Railway, The Korean Physical Society, Vol. 69, No. 4, pp.361-368.
12. Harold A. Sabbagh, Elias H. Sabbagh, R. Kim Murphy (2002) Recent advances in modeling eddy-current probes, AIP Conference Proceedings, Vol. 615, No.1
13. Noritaka Yusa, Stephane Perrin, Kazue Mizuno, Zhenmao Chen, Kenzo Miya (2007) Eddy current inspection of closed fatigue and stress corrosion cracks, Measurement Science and Technology, Vol. 18, No.11

14. H. J. Lee, Y. S. Kim M. W. Nam, B. S. Y, S. K. Kim (1999) Eddy Current Testing of Weldment by Plus(+) Point Probe, Journal of the Korean Society Nondestructive Testing, Vol. 19, No. 6, pp.426-432.
15. S. J. Min (2015) An Optimum Maintenance for Rail Surface Considering Dynamic Wheel-rail Force, Master thesis.
16. R.S. Dwyer-Joyce, R. Lewis, N. Gao, D. G. Grieve (2003) Wear and Fatigue of Railway Track Caused by Contamination, Sanding and Surface Damage, White Rose Research Online, pp.211-220.